

Hybrid RF-mmWave Communications to Achieve Low Latency and High Energy Efficiency in 5G Cellular Systems

Morteza Hashemi, C. Emre Koksal, and Ness B. Shroff

Department of Electrical and Computer Engineering, The Ohio State University, Columbus, OH

Abstract—We propose a hybrid architecture to integrate RF (i.e., sub-6 GHz) and millimeter wave (mmWave) interfaces for 5G cellular systems. To alleviate the challenges associated with mmWave communications, our proposed architecture integrates the RF and mmWave interfaces for *beamforming* and *data transfer*, and exploits the spatio-temporal correlations between the interfaces. Based on extensive experimentation in indoor and outdoor settings, we demonstrate that an integrated RF/mmWave signaling and channel estimation scheme can remedy the problem of high training overhead associated with mmWave beamforming. In addition, cooperation between two interfaces at the higher layers effectively addresses the high delays caused by highly intermittent connectivity in mmWave channels. Subsequently, we formulate an optimal scheduling problem over the RF and mmWave interfaces where the goal is to maximize the delay-constrained throughput of the mmWave interface. We prove using subadditivity analysis that the optimal scheduling policy is based on a single threshold that can be easily adopted despite high link variations. We design an optimal scheduler that opportunistically schedules the packets over the mmWave interface, while the RF link acts as a fallback mechanism to prevent high delay.

I. INTRODUCTION

The annual data traffic generated by mobile devices is expected to surpass 130 exabits by 2020 [1]. This deluge of traffic will significantly exacerbate the spectrum crunch that cellular providers are already experiencing. To address this issue, it is envisioned that in 5G cellular systems certain portions of the mmWave band will be used, spanning the spectrum between 30 GHz to 300 GHz [2]. However, before mmWave communications can become a reality, there are significant challenges that need to be overcome. Compared with the RF bands (i.e., sub-6 GHz), the propagation loss in the mmWave band is much higher due to atmospheric absorption and low penetration. Although large and highly directional antenna arrays can potentially make up for the propagation losses, they cause several other issues such as high energy consumption by components (e.g., analog-to-digital (A/D) converters). Moreover, in order to fully utilize the directional antenna arrays, continuous beamforming and signal training at the receiver is needed [3]. Digital beamforming is highly efficient in delay, but there is a need for a separate A/D converter for each antenna, which may not be feasible due to high energy consumption. In contrast, analog beamforming requires only one A/D, but it can focus on one direction at a time, making the search process costly in delay. There are also proposals on hybrid digital/analog beamforming [4], which strikes a balance between analog and digital beamforming.

In addition to the need for an efficient beamforming approach, a given mmWave channel can be highly variable with intermittent connectivity since most objects lead to blocking

and reflections as opposed to scattering and diffraction in typical RF frequencies. Moreover, due to mobile users and dynamic surrounding objects, different propagation paths become highly variable with intermittent on-off periods. This can result in long outages and poor mmWave delay performance.

In this paper, we propose a hybrid RF/mmWave architecture in which the RF interface is used for beamforming as well as data transfer. Due to high cost and energy consumption by A/D converters in fully-digital beamforming as well as the delay in fully-analog beamforming, we investigate the feasibility of conducting a coarse angle of arrival (AoA) estimation on the RF channel and then utilizing the fully-analog beamforming for fine tuning and transmission. To this end, we first experimentally verify the correlation between the RF and mmWave AoA, especially in the presence of line-of-sight (LOS). Our measurements taken jointly at different bands and for both *indoor and outdoor settings* show that under LOS conditions and in 94% of measurements, the identified AoA of signal in the RF band is within $\pm 10^\circ$ accuracy for the AoA of the mmWave signal. Based on the estimated RF AoA, the angular range over which we scan for the mmWave transmitter reduces to no more than 20° on average, from 180° in stand-alone mmWave systems. The authors in [5] have also proposed a beamforming method based on out-of-band measurements for 60 GHz WiFi and under *static indoor* conditions.

Next, we investigate an RF-assisted mmWave communications, in which, in addition to beamforming, the RF interface is used for data transfer. The mmWave interface is different from classical wireless interfaces in which data rates are much smaller than the clock speeds of the processors. In contrast, the link speeds of the mmWave interface (multi-Gbps) are comparable to the speed at which a typical processor in a smart device operates. Thus, for mmWave, the wireless interface cannot be assumed to operate at smaller time-scales and the algorithms run at the processor may not be able to respond to variations in real time and execute control decisions. *This necessitates the use of a reasonably large buffer at the mmWave interface along with proactive queue-control solutions.* For instance, if the queue size at the mmWave interface gets small, the risk of wasting the abundant capacity from mmWave increases. Conversely, if we keep the queue at the mmWave interface large, if the channel goes down, we incur a high delay.

To understand the tradeoff between full exploitation of the mmWave capacity and the delay for mmWave channel access, we model the hybrid RF/mmWave transceiver as a network, and study an optimal scheduling problem where the goal is to achieve maximum mmWave channel utilization with a bounded

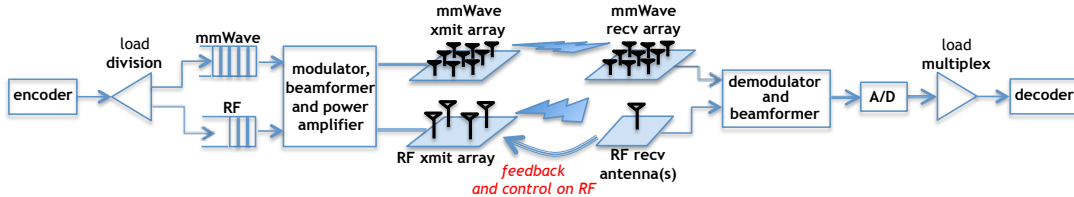


Fig. 1. Our hybrid communication system. The speed of mmWave interface necessitates the use of a separate queue at the input of that interface. RF antenna arrays are needed at the access points and not necessary at the mobiles.

delay. In order to determine “when” a data packet should be added to the RF or mmWave queues, we prove that the optimal policy is of the *threshold-type* such that the scheduler routes the arrival traffic to the mmWave queue if and only if its queue length is smaller than a threshold. We show that the threshold-based scheduling policy efficiently captures the dynamics of the mmWave channel, and indeed maximizes the channel utilization. Our main contributions are the following:

- We have conducted a wide variety of experiments to evaluate the correlation between the measured channel gains for the 30 GHz mmWave and 3 GHz RF interfaces under various indoor and outdoor situations involving existence of LOS between the transmitter and receiver.
- We propose a hybrid RF/mmWave system that exploits the cross-interface correlations for beamforming and data transfer. Our A/D follows the beamformer at the receiver, and eliminates the need for a separate A/D for each element in the mmWave antenna-array.
- We propose a framework to jointly manage the queues at the RF and mmWave interfaces. Our queue management formulation explicitly takes into account the mmWave channel dynamics, and our approach enables full utilization of the available mmWave channel capacity, despite the highly variable nature of the channel. We prove using subadditivity analysis that the optimal scheduling policy is a simple threshold based one, which can be easily adopted despite the high link variations.

We should emphasize that the RF/mmWave correlation was studied in [6], and applied only for beamforming in [5]. However, a coherent design that fully integrates the RF and mmWave interfaces is lacking. Hence, we aim to develop a hybrid architecture for which the RF interface is utilized for both beamforming and data transfer.

Notations: We use the following notation throughout the paper. Bold uppercase and lowercase letters are used for matrices and vectors, respectively, while non-bold letters are used for scalars. In addition, $(\cdot)^\dagger$ denotes the conjugate transpose, $\text{tr}(\cdot)$ denotes the matrix trace operator, and $\mathbb{E}[\cdot]$ denotes the expectation operator. The RF and mmWave variables are denoted by $(\cdot)_{\text{RF}}$ and $(\cdot)_{\text{mm}}$, respectively.

II. RELATED WORK

We classify related work across the following thrusts:

1) *Experimental investigations:* There exist numerous measurement and experimentation efforts in order to understand mmWave propagation and the effect of slow scale and large scale fading in the mmWave band (see, for example, [2, 7]). The main objective has been to extend the existing far-field

ray-tracing models to accurately represent various phenomena observed in mmWave. Our goal is to neither replicate nor expand these observations. Instead, we are interested in the channel/propagation environment correlation across different interfaces under various conditions, including indoor and outdoor situations, with mobility, and existence of line-of-sight.

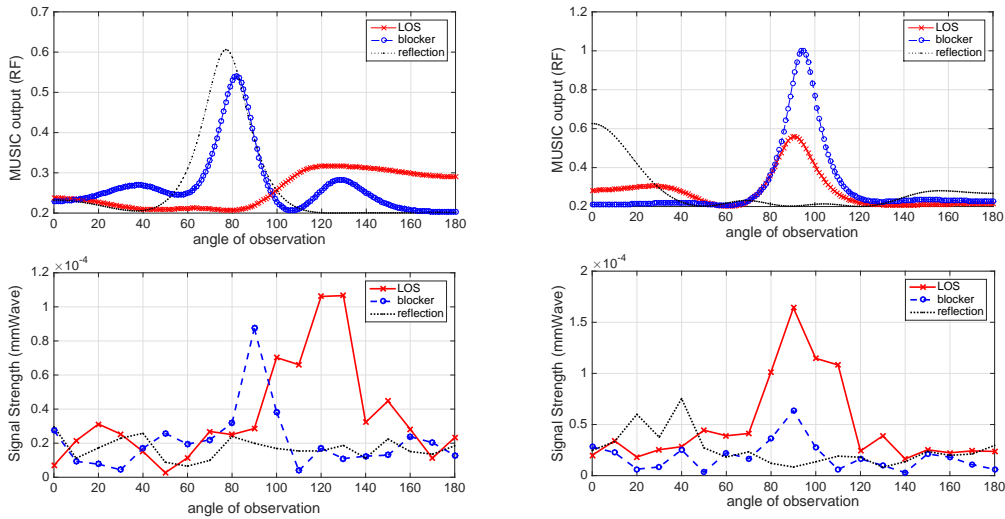
2) *Dual-interface beamforming and communications:* There has been extensive amount of work on digital and analog beamforming methods (e.g., [3, 8]). There are also proposals on hybrid beamforming methods [4] in which the term “hybrid” refers to the mixture of analog/digital (different from our hybrid RF/mmWave system). The authors in [5] proposed a beam steering method for *indoor* 60 GHz WiFi using legacy WiFi measurements. That work investigated delay overhead reduction in beam steering using out-of-band measurement. Similarly, the authors in [6] provided a transform method that can be used to relate the spatial correlation matrix derived at one frequency to another much different frequency. In the context of hybrid communications and data transfer, the authors in [9] studied a dual interface system to offload cellular data over WiFi.

Compared with the existing work, our contribution is twofold: (i) we experimentally investigate the RF/mmWave correlation under practical scenarios, and demonstrate that how mobility affects the channel conditions and cross-interface correlation, and (ii) we propose a holistic RF/mmWave architecture wherein the RF interface is exploited for beamforming as well as data transfer in order to reduce energy consumption and prevent high delay caused by mmWave outages.

III. SYSTEM MODEL

A. Architecture Model

One of the main drivers behind the emergence of mmWave mobile communications is the recent advances in antenna technology that allow deployment of large antenna arrays in relatively small chip areas. Although such arrays can make up for the high losses in the mmWave band, they cause several other issues such as high energy consumption. For instance, at a sampling rate of 1.6 Gsamples/sec, an 8-bit quantizer consumes $\approx 250\text{mW}$ of power. During active transmissions, this would constitute up to 50% of the overall power consumed for a typical smart phone. In order to alleviate the challenges associated with mmWave systems, Fig. 1 illustrates the basic components of the proposed hybrid architecture that exploits the correlation between the mmWave and RF channels as it pertains to large-scale effects and AoA in the presence of LOS path [5, 6]. In this model, beamforming is achieved fully in the analog domain and thus only one A/D is needed, while the cross-interface correlation addresses the delay issue of



(a) RF and mmWave activity vs. angle in *indoor* setting (b) RF and mmWave activity vs. angle in *outdoor* setting

Fig. 2. Indoor (2(a)) and outdoor (2(b)) associated with RF (top plots) and mmWave (bottom plots). In each case, we have tested three situations: LOS, blocker, and NLOS with reflector. The direction of strong signal is highly correlated between RF and mmWave if a LOS is present. The correlation is lost in part, if there is a blocker present and lost completely in the case of NLOS with reflections.

analog beamforming. Moreover, all mmWave control signaling and channel state information (CSI) are moved to RF and thereby it avoids the two-way beamforming and reverse channel transmission costs in mmWave.

B. Channel Model

In Fig. 1, we use digital and analog beamforming for the RF and mmWave interfaces, respectively. A snapshot¹ of the received signals at both interfaces can be written as:

$$\mathbf{y}_{\text{RF}} = \mathbf{H}_{\text{RF}} \cdot \mathbf{x}_{\text{RF}} + \mathbf{n}_{\text{RF}} \quad \text{and} \quad y_{\text{mm}} = \mathbf{w}_r^\dagger \mathbf{H}_{\text{mm}} \mathbf{w}_t \cdot x_{\text{mm}} + n_{\text{mm}}, \quad (1)$$

where \mathbf{H}_{RF} is the RF-channel matrix, and \mathbf{x}_{RF} is the transmitted signal vector in RF. Unlike RF, we use analog combining for mmWave via a single A/D, where \mathbf{w}_r and \mathbf{w}_t are the analog-receive and digital-transmit beamforming vectors. Consequently, the signal at the input of the decoder is a scalar, identical to a weighted combination of signal x_{mm} across all antennas. *Note that, our formulation can readily be extended to the case with digital combining at mmWave, in case A/D conversion is made at the output of each antenna.* Entries of circularly symmetric white Gaussian noise are denoted by \mathbf{n}_{RF} and n_{mm} . The RF receiver uses the steering vector $\mathbf{w}_{\theta_{\text{RF}}}$ to align the received signals where the optimal steering direction θ_{RF}^* can be obtained based on maximizing the SNR, i.e.,:

$$\theta_{\text{RF}}^* = \arg \max_{\theta_{\text{RF}}} \frac{\mathbf{w}_{\theta_{\text{RF}}}^\dagger \mathbf{H}_{\text{RF}} \mathbf{K}_{x,x} \mathbf{H}_{\text{RF}}^\dagger \mathbf{w}_{\theta_{\text{RF}}}}{N_0},$$

where $\mathbf{K}_{x,x}$ is the covariance matrix, and N_0 is the noise power.

In the mmWave domain, the channel matrix \mathbf{H}_{mm} has a singular value decomposition $\mathbf{H}_{\text{mm}} = \mathbf{U} \mathbf{\Lambda} \mathbf{V}^\dagger$, where $\mathbf{U} \in \mathcal{C}^{n_r \times n_r}$ and $\mathbf{V} \in \mathcal{C}^{n_t \times n_t}$ are rotation unitary matrices and $\mathbf{\Lambda} \in \mathcal{R}^{n_r \times n_t}$ is a diagonal matrix whose diagonal elements are nonnegative real numbers $\rho_1 \geq \rho_2 \geq \dots \geq \rho_{n_{\text{min}}}$, where $n_{\text{min}} = \min(n_r, n_t)$. The mmWave-channel matrix \mathbf{H}_{mm} is low rank [10], and since the rank of \mathbf{H}_{mm} is equal to the number of non-zero singular values, we restrict our attention to only the largest eigenvalue

ρ_1 and assume that $\rho_1 \gg \rho_i$, and that $\rho_i \approx 0$ for $i \neq 1$. In fact, our experimental results show that under the LOS conditions, there is about 10 – 15 dB gain improvement due to the strongest eigenmode, and thus we assume that the state of link can be characterized based on the value of ρ_1 . Next, we experimentally investigate the correlation between the RF and mmWave channels under various conditions.

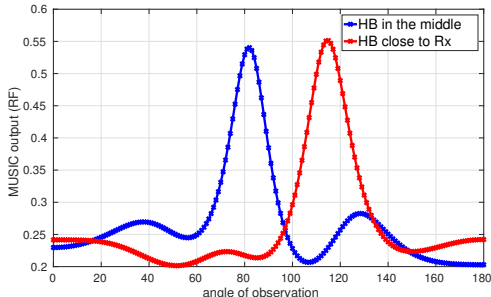
C. Experimental Observations

We simultaneously observe the RF and mmWave channels via a dual transmitter-receiver pair in the same location. In the RF platform, we use an omni-directional antenna operating at 3 GHz as a transmitter and 5 omni-directional antennas as a receiver in order to observe the AoA for the incoming RF signal. We use the MUSIC algorithm² [11] to evaluate the components of the signals across various angles. For mmWave, we use 30 GHz directional antennas to be able to align the beams. We measure the channel across the 180° space with 10° step size. Based on a large set of measurements, we conclude that the propagation situations can be classified into three types as it pertains to summarizing the connection between the large-scale effects in RF and mmWave: line-of-sight (LOS), blocker, and non line-of-sight (NLOS). LOS implies that there is a strong line of sight path between the transmitter and the receiver; blocker indicates that, the LOS path for the mmWave interface is being blocked by a non-stationary obstacle; and NLOS indicates the presence of a stationary obstacle, unlikely to change in time.

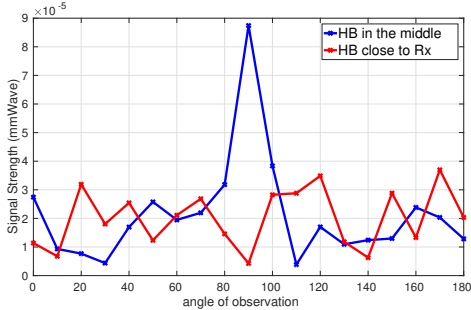
Figure 2 provides our *indoor and outdoor* measurement results, taken simultaneously for RF and mmWave. The output of the MUSIC algorithm is given on the top plots, and the important thing to focus on is the correct AoA in each situation. Note that the AoA is different across different observations plotted. Once that AoA is identified, we compare it with the signal strength (bottom plots) we measured along that direction

¹To avoid cumbersome notations, time dependency has been dropped.

²For the sake of clarity, we use MUSIC algorithm, but other estimators can be used as well.



(a) RF activity vs. angle in indoor setting



(b) mmWave activity vs. angle in indoor setting

Fig. 3. Channel spatial behavior for human block (HB) in indoor environment for RF (top) and mmWave (bottom).

for the mmWave signal generated at the transmitter location as the RF signal. For the LOS situation, for both indoor and outdoor, there is a strong correlation in the angular composition and the strength of signal coming across all angles in RF and mmWave. This observation is in agreement with [5]. Indeed, in 94% of all measurements, we have identified the AoA predicted by MUSIC within a $\pm 10^\circ$ accuracy for the AoA of the mmWave signal. As a result, based on RF measurements, the correct mmWave transmitter location can be almost perfectly identified under LOS. From Fig. 2, it is evident that as we lose the LOS, the RF/mmWave correlation is lost and the signal strength in mmWave starts to drop rapidly. However, depending on the size and the location of the blocker, AoA estimation accuracy varies. For instance, for a small/mid-size blocker in the middle, in 55% of the observations do the RF and mmWave signals have their strongest paths within $\pm 10^\circ$ of each other. Figure 3 demonstrates the effect of human blocker located in the middle compared with when the blocker moves very close to the receiver. From the results, we note that as the blocker moves towards the receiver, the correlation decreases.

Our major experimental observation is that in LOS situations, there is a high correlation between the observed RF and mmWave signals, both in signal strength and AoA. Therefore, LOS instances should be exploited in mmWave as much as possible, since there is an associated 10 – 15 dB channel gain improvement as well. In order to detect LOS situations, Fig. 4 illustrates the spatial variations of the mmWave channel gain in LOS and reflection situations. We observe that the LOS situation is quite robust with respect to slight movements, i.e., the large-scale effects lead to minor variations in the channel gain, if the presence of LOS is preserved. On the other hand, if the LOS is blocked and the connection depends on a

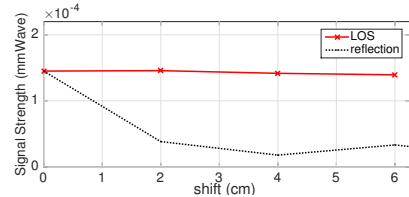


Fig. 4. Spatial variation in the channel gain. Small movements lead to significant variations without LOS.

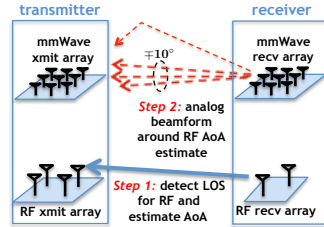


Fig. 5. Our beamformer works in two phases: (1) the presence of LOS is detected and AoA is estimated all in RF; (2) analog mmWave beamformer focuses on a small area around the estimated AoA.

strong reflector, channel gain becomes relatively unstable and slight movements can result in drastic changes in the channel. As a result, we use the sensitivity of channel gain to slight movements in order to predict the loss of LOS and take the necessary precautions for a smoother transition in order to mitigate the negative effects of connection losses on the user experience. The authors in [5] use the ratio of the highest signal strength component to the average received signal energy (i.e., peak to average power ratio (PAPR)) as an indicator for LOS inference. Under mobility, the PAPR can be paired with our indicator to boost the LOS detection accuracy.

D. Beamforming

The mmWave channel is often sparse in the angular domain, with a few scattering clusters, each with several rays, in addition to a dominant LOS path [10]. Thus, in order to find the optimal mmWave steering direction θ_{mm}^* , our proposed architecture exploits the correlation between the RF and mmWave AoA. We use a coarse AoA estimation on the RF channel and then utilize analog beamforming for fine tuning around the estimated AoA. The RF/mmWave AoA correlation reduces the angular search space, and thus addresses the delay issue of fully-analog beamforming. The algorithm is specified below, and is graphically illustrated in Fig. 5.

- 1) Start the system in the **RF-only** mode.
- 2) Implement MUSIC algorithm in RF and estimate the angle of arrival A_{RF} based on beacons.
- 3) Use analog beamforming to fine tune the mmWave beam in the range of $A_{RF} \pm 10^\circ$:
 - a) If the LOS is detected, both interfaces operate jointly in the **dual RF/mmWave mode** in which resources and arrival traffic are allocated jointly.
 - b) Otherwise, continue operation of the system in the **RF-only** mode.
- 4) Go to Step (2) after every T seconds wherein T is a recalibration system parameter.

Remark 1: As our experimental results show, the RF/mmWave correlation decreases as the LOS condition is lost. However, the RF-assisted beamforming relies on the cross-interface correlation, and once the correlation is lost, it falls back to the traditional beamforming schemes.

Remark 2: The parameter of searching $\pm 10^\circ$ around the estimated AoA is set based on our experimental setup. In general, it will be configured based on dynamics of the scenario and antenna beamwidth.

IV. RF-ASSISTED MMWAVE COMMUNICATIONS

In the proposed hybrid architecture, once the dual RF/mmWave mode is activated, the load division component (in Fig. 1) schedules the arrival traffic over the RF and mmWave interfaces. The goal is to achieve maximum mmWave throughput while its delay is guaranteed to be bounded. We use network optimization tools to optimize the hybrid transceiver design. To this end, we model our hybrid RF/mmWave transceiver as a *diamond network* (see Fig. 7) in which each of the RF and mmWave interfaces are represented by a separate node. Moreover, a virtual destination (i.e., receiver) node d has been added, and since all data packets are destined for node d , its queue length, $Q_d(t)$, is set to be 0 for all t .

A. Network Model

We assume that the system evolves in discrete (slotted) time $t \in \{0, 1, 2, \dots\}$, and there is an exogenous packet arrival process with rate λ . To quantify the behavior of the mmWave link using the strongest eigenmode (i.e., corresponding to ρ_1), a two-state model (outage and non-outage) can be used. The probability of being in each state is a function of distance, and statistical models can be fit [2]. Therefore, we assume that the binary process $\{L(t)\}_{t=1}^\infty$ accounts for mmWave outage and non-outage situations, such that $L(t) := 1$ implies the availability of the mmWave link (i.e., non-outage or ON state) during time slot t and $L(t) := 0$ otherwise (i.e., outage or OFF state). As we also experimentally show in Section V (see Fig. 9), $L(t) = 1$ corresponds to LOS situations, while $L(t) = 0$ can be mapped to the NLOS situations like human blockers or when there are no strong reflectors. We further assume that T_n^{on} and T_n^{off} (with general random variables T_{on} and T_{off}) denote the n -th ON and OFF periods respectively, as shown in Fig. 6. The sequence of ON times $\{T_n^{\text{on}} : n \geq 1\}$ and OFF times $\{T_n^{\text{off}} : n \geq 1\}$ are independent sequences of i.i.d positive random variables. Unlike mmWave, the RF link is much less sensitive to blockage due to diffraction. Thus, for the sake of simplicity, we assume that the RF link is available during all time slots even when $L(t)$ takes on the value of 0.

The dynamics of the mmWave link during time slot t is denoted by $\mathbf{x}(t) = (Q(t), D(t))$ in which $Q(t)$ is the mmWave queue length, and $D(t)$ is the waiting time of the head-of-line packet in the mmWave queue³. The state space is denoted by \mathcal{S} , and a scheduling policy $\pi \in \Pi$ determines the assignment of packets to the mmWave or RF queue, i.e., $\pi : \mathcal{Q} \rightarrow \{0, 1\}$ in

³For the sake of notations, we drop the subscript $(\cdot)_{\text{mm}}$ from the mmWave variables.

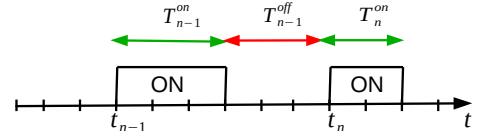


Fig. 6. ON-OFF periods of the mmWave link availability

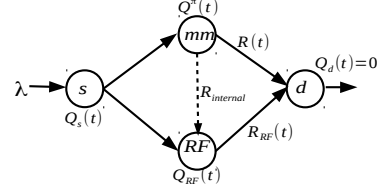


Fig. 7. An equivalent network model for the hybrid RF/mmWave transceiver in which mmWave (denoted by m) and RF (denoted by r) interfaces are viewed as individual nodes of the network.

which Π denotes the class of *feasible causal* policies in a sense that scheduling decisions are made based on current state. The decision variable $\pi(Q(t)) = 1$ (or, in short, $\pi = 1$) implies that the packet is routed to the mmWave queue, and $\pi(Q(t)) = 0$ (or $\pi = 0$) implies that the packet is routed to the RF queue. The number of packets added to the mmWave queue at time slot t is denoted by $\beta^\pi(t)$. To avoid a large waiting time in the mmWave queue due to intermittent connectivity, we require the packets to be *impatient* in the sense that if the waiting time of the head-of-line packet in the mmWave queue exceeds a timeout T_{out} , the packet “reneges” (is moved to) to the RF queue, i.e., if $D(t) \geq T_{\text{out}}$ holds. In order to account for packets reneging, we consider a “virtual” link between the mmWave and RF queues with a rate equal to the internal read/write speed of processor, as shown in Fig. 7. In this case, $\gamma^\pi(t, T_{\text{out}})$ denotes the number of reneged packets and $\alpha^\pi(t)$ is the number of packets that are completely served by the mmWave interface at time t . Therefore, the mmWave queue evolves as: $Q^\pi(t) = \max[0, Q^\pi(t-1) + \beta^\pi(t) - \alpha^\pi(t) - \gamma^\pi(t, T_{\text{out}})]$.

B. Problem Formulation

Definition 1 (Average throughput and reneging rate) Under the scheduling policy π with timeout T_{out} , given that $\alpha^\pi(t)$ packets are completely served by the mmWave queue, and $\gamma^\pi(t, T_{\text{out}})$ packets renege at time slot t , the average throughput and reneging rate of the policy π is defined as:

$$\bar{\alpha}(\pi) = \limsup_{T \rightarrow \infty} \frac{1}{T} \mathbb{E} \left[\sum_{t=0}^T \alpha^\pi(t) \right], \quad (2)$$

$$\bar{\gamma}(\pi, T_{\text{out}}) = \limsup_{T \rightarrow \infty} \frac{1}{T} \mathbb{E} \left[\sum_{t=0}^T \gamma^\pi(t, T_{\text{out}}) \right]. \quad (3)$$

In order for the expectations in (2) and (3) to exist, we assume that $\alpha^\pi(t)$ and $\gamma^\pi(t, T_{\text{out}})$ are stationary ergodic. In this model, imposing the service deadline T_{out} ensures that the average waiting time of the mmWave queue is smaller than or equal to T_{out} . Hence, the reneging mechanism explicitly dictates a constraint on the mmWave waiting time. Our goal is to derive a throughput-optimal policy with a constrained reneging rate.

Problem 1 (Constrained Throughput Optimization) Given that there is a timeout T_{out} for packets in the mmWave queue, Problem 1 is defined as:

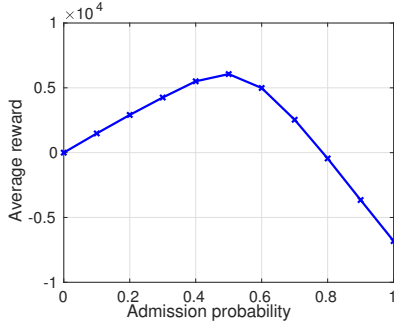


Fig. 8. Probabilistic admission policy

$$\begin{aligned} & \max_{\pi \in \Pi} \bar{\alpha}(\pi) \\ & \text{s.t. } \bar{\gamma}(\pi, T_{out}) \leq \epsilon \text{ and } \bar{\beta}(\pi) \leq \lambda, \end{aligned} \quad (4)$$

for a given $\epsilon < \lambda$. The objective function and the first constraint can be relaxed as: $\max_{\pi \in \Pi} \bar{\alpha}(\pi) - b(\bar{\gamma}(\pi, T_{out}) - \epsilon)$, where b is a positive Lagrange multiplier. For any particular fixed value of b , it is straightforward to show that there is no loss of optimality in the relaxed problem. Moreover, we note that the relaxed formulation can be interpreted as an optimization over obtained *rewards* and paid *costs*. In particular, we assume that each packet that receives service from the mmWave link, results in r units of reward (i.e., in terms of mmWave throughput), while a packet reneging incurs a cost of c (i.e., in terms of wasted waiting time in the mmWave queue). Therefore, we can model Problem 1 as a reward optimization problem.

Problem 2 (Total Reward Optimization) We consider the maximization problem over total rewards obtained as a result of serving packets, and costs due to packets reneging, i.e.,:

$$\begin{aligned} & \max_{\pi \in \Pi} \limsup_{T \rightarrow \infty} \frac{1}{T} \mathbb{E} \left[\sum_{t=0}^T r\alpha^\pi(t) - c\gamma^\pi(t, T_{out}) \right] \\ & \text{s.t. } \limsup_{T \rightarrow \infty} \frac{1}{T} \mathbb{E} \left[\sum_{t=0}^T \beta^\pi(t) \right] \leq \lambda, \end{aligned} \quad (5)$$

where the constraint $\bar{\alpha}(\pi) \leq \bar{\beta}(\pi)$ is implicit. It is straightforward to show that an optimal solution π^* for the relaxed formulation of Problem 1 is the optimal solution for (5) and vice versa. For instance, for $r = 1$ and $c = b$, two formulations will be identical. In general, the values of r and c are set based on the application and performance requirements. Specifically, a large value of r ensures high throughput, while a large value of c prioritizes low-latency performance (i.e., a *conservative policy*). Therefore, (5) captures the tradeoff between full exploitation of the mmWave capacity and the delay for mmWave channel access through the control knob $\beta^\pi(t)$: if $\beta^\pi(t)$ is set to a very small value for all time slots t (i.e., a conservative policy) then $\alpha^\pi(t)$ would be small as well, and the objective function reduces due to the first term. On the other hand, if $\beta^\pi(t)$ is set to a large value (e.g., matched to the arrival rate λ for all time slots t) and the link state fluctuates according to the process $\{L(t)\}_{t=1}^\infty$, then the objective function could decrease due to the reneging cost that is captured by the second term. Therefore, there is an optimal value of $\beta^\pi(t)$ within these two extreme cases that results in the maximum return rate. For instance, Fig. 8 demonstrates behavior of the objective function in (5) under a

probabilistic admission policy by which the input arrival rate λ is admitted to the mmWave queue with an admission probability p . In this case, the objective value increases by admitting more packets into the queue up to a certain threshold, and thereafter the objective value decreases due to the dominant reneging cost.

C. Optimal RF/mmWave Scheduling Policy

From (5) and using the Lagrangian relaxation, we define:

$$\begin{aligned} g(W) &= \max_{\pi \in \Pi} \left[r\bar{\alpha}(\pi) - c(\bar{\beta}(\pi) - \bar{\alpha}(\pi)) + W(\lambda - \bar{\beta}(\pi)) \right] \\ &= \max_{\pi \in \Pi} \left[(r+c)\bar{\alpha}(\pi) + (W+c)(\lambda - \bar{\beta}(\pi)) \right] - c\lambda, \end{aligned} \quad (6)$$

in which the Lagrange multiplier W is positive, and it can be interpreted as a *subsidy* for taking the passive action. In our problem, the active action corresponds to admitting packets in the mmWave queue, and passive action is equivalent to adding packets into the RF queue. Hence, the goal is to maximize the long-term expected reward by balancing the reward for serving and the subsidy for passivity. Note that the solution of (6) partitions the state space \mathcal{S} into three sets, \mathcal{S}_0 , \mathcal{S}_1 and \mathcal{S}_{01} , where, respectively, the optimal action is $\pi(\mathbf{x}) = 0$ for $\mathbf{x} \in \mathcal{S}_0$, $\pi(\mathbf{x}) = 1$ for $\mathbf{x} \in \mathcal{S}_1$, or some randomization between both $\pi(\mathbf{x}) = 0$ and $\pi(\mathbf{x}) = 1$ for $\mathbf{x} \in \mathcal{S}_{01}$ [12]. Moreover, it is known that in a Markov Decision Process if the state space contains a finite number of states, which holds in our model, then the set \mathcal{S}_{01} does not contain more than one state. The following Theorem states that Problems 1 and 2 are solved by a *monotone policy*: a class of policies Π has monotone structure if for $\pi \in \Pi$, there exists $y \in \{1, 2, \dots, K\}$ such that: $\pi(Q) = 0 \iff Q \geq y$.

Theorem 1. (Optimality of monotone policy) The solution for the reward optimization in (6) has a monotone structure.

Proof. Let us denote by $v(Q, D)$, the value function corresponding to Problem 2 when mmWave is at state (Q, D) , and $V(Q) = \sum_{1 \leq D \leq T_{out}} v(Q, D)$. From the Bellman equation [12], we have:

$$\begin{aligned} g(W) &= V(Q) + \max \left\{ \lambda V(Q+1) + \sigma Q V(Q-1) + \right. \\ & \quad \left. \mu V(Q-1), W + \sigma Q V(Q-1) + \mu V(Q-1) \right\}, \end{aligned} \quad (7)$$

in which, σ is the reneging rate and μ is the mmWave service rate. We prove that if passive action is optimal in Q then passive action is optimal in $Q' \geq Q$. Similar to [13], let us define:

$$\begin{aligned} f(Q, 0) &= r + W + \mu V(Q-1) + \sigma Q V(Q-1); \\ f(Q, 1) &= r + \lambda V(Q+1) + \sigma Q V(Q-1) + \mu V(Q-1), \end{aligned}$$

and $\varphi(Q) = \arg \max_{a \in \{0,1\}} f(Q, a)$. It then suffices to show that $\varphi(Q') \leq \varphi(Q)$ for $Q' \geq Q$. Assuming $a \leq \varphi(Q')$, we have $f(Q', \varphi(Q')) - f(Q', a) \geq 0$. Let us now prove that $V(Q)$ has the *subadditivity* property.

Definition 2 (Subadditive function) Let X and Y be partially ordered sets and $u(x, y)$ a real-valued function on $X \times Y$. We say that u is subadditive if for $x^+ \geq x^-$ in X and $y^+ \geq y^-$ in Y we have: $u(x^+, y^+) + u(x^-, y^-) \leq u(x^+, y^-) + u(x^-, y^+)$.

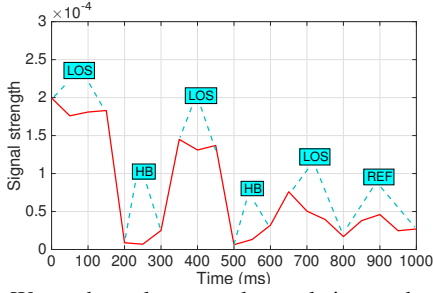


Fig. 9. MmWave channel temporal correlation under line of sight (LOS), human block (HB), and reflection (REF)

To prove that $V(Q)$ is a subadditive function, it suffices to show that for all $Q' \geq Q$ and $a \in \{0, 1\}$, the inequality $f(Q', a) + f(Q, \varphi(Q')) \leq f(Q', \varphi(Q')) + f(Q, a)$ holds. If $\varphi(Q') = a = 0$ or $\varphi(Q') = a = 1$, then the inequality is satisfied. If $\varphi(Q') = 1$ and $a = 0$, then we show that $f(Q, 1) - f(Q, 0) \leq f(Q', 1) - f(Q', 0)$, or equivalently, $\lambda V(Q + 1) \leq \lambda V(Q' + 1)$. This inequality is true due to the fact that $V(\cdot)$ is non-decreasing, and thus the theorem statement follows. Note that $V(Q)$ is a function of reward and channel state, and it is proportional to the number of packets in the mmWave queue. \square

Intuitively, for a first-in-first-out (FIFO) queue, the likelihood that an admitted packet reneges before receiving service increases with the number of queued packets. Therefore, given that the renegeing and moving packets from the mmWave queue to the RF queue incurs a delay cost, it is in the scheduler interest to exercise admission control and deny entry to packets when the mmWave queue grows and becomes larger than a threshold. Next we characterize the value of optimal threshold.

Optimal threshold: The optimal policy π^* imposes a threshold $h^* \in \{0, 1, 2, \dots\}$ such that $\pi^* = 1$ if and only if $Q < h^*$. Under the ergodicity assumption, we rewrite Problem 2 as:

$$\max_{h \in \{0, 1, 2, \dots\}} \left((r + c) \mathbb{E}[\alpha_h] - (W + c) \mathbb{E}[\beta_h] \right). \quad (8)$$

The following theorem specifies the optimal admission threshold h^* similar to the method used in [13].

Theorem 2. Given an admission threshold h , we define

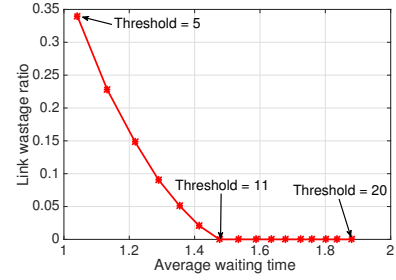
$$\phi(h) := (W + c) \frac{\mathbb{E}[\beta_h] - \mathbb{E}[\beta_{h-1}]}{\mathbb{E}[\alpha_h] - \mathbb{E}[\alpha_{h-1}]}. \quad (9)$$

If $\phi(h) < r + c \leq \phi(h + 1)$, then $h^* = h$.

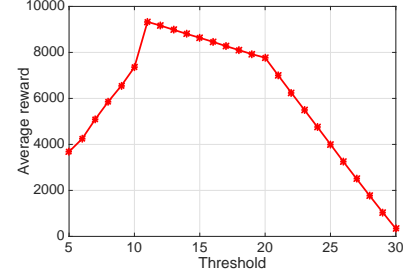
Proof. Due to space limitations, we provide a sketch of proof. Details are available in our online technical report [14]. In particular, we can show that $\phi(h)$ is non-decreasing in h , i.e., $\phi(h - 1) \leq \phi(h), \forall h > 1$. For a threshold h that satisfies $r + c \leq \phi(h + 1)$, we can see $(r + c) \mathbb{E}[\alpha_{h+1}] - (W + c) \mathbb{E}[\beta_{h+1}] \leq (r + c) \mathbb{E}[\alpha_h] - (W + c) \mathbb{E}[\beta_h]$. Therefore, h achieves a higher objective value than $h + 1$. Now in order to establish this result for $h + 2$, we can show that:

$$r + c \leq \phi(h + 1) \leq \phi(h + 2) \leq (W + c) \frac{\mathbb{E}[\beta_{h+2}] - \mathbb{E}[\beta_h]}{\mathbb{E}[\alpha_{h+2}] - \mathbb{E}[\alpha_h]},$$

from which we conclude that h is optimal with respect to $h + 2$ as well. By induction, we extend this result for all



(a) Tradeoff between delay and link wastage ratio



(b) Total reward obtained as a function of threshold

Fig. 10. (a) Trade-off between the average waiting time and link wastage. The control knob is the admission threshold (b) Performance of our proposed framework that maximizes total reward. The optimal threshold results in zero wastage and the lowest delay in Fig. (a).

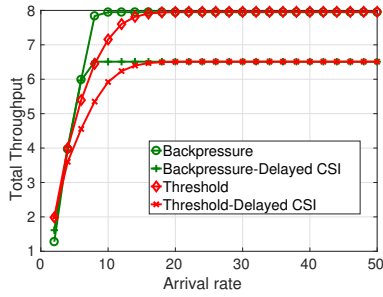
$h' > h$. Similarly, based on the constraint $\phi(h) < r + c$ we prove that h is optimal with respect to all $h' < h$ as well. Thus, h is the optimal threshold value in general, and we have $h^* = h$. Note that $\mathbb{E}[\beta_h] = \lambda \sum_{Q < h, D} \xi_{(Q, D)}$ and $\mathbb{E}[\alpha_h] = \mathbb{E}[\beta_h] - \sigma \sum_{Q, D = T_{out}} \xi_{(Q, D)}$, with reneging rate σ and $\xi_{(Q, D)}$ to be limiting probability of the state $\mathbf{x} = (Q, D)$. Details of the limiting distribution and *online* calculation of h^* are provided in our technical report [14]. \square

We can show that the value of optimal threshold in fact increases with respect to r , and decreases in c [14]. Hence, if the value of r increases, throughput performance will have a higher priority than delay, and thus optimal threshold increases, as expected. On the other hand, by increasing the value of c , the optimal threshold decreases to avoid high reneging costs.

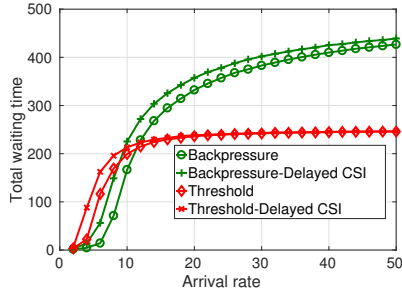
V. NUMERICAL RESULTS

We use experimentation to generate traces for the ON-OFF mmWave link model. In particular, a mobile receiver moves with the speed of 1m/s over a path characterized by sudden link transitions due to human blockers (HB) and reflectors (REF). Figure 9 illustrates the received signal strength as the mobile moves away from the transmitter. We assume a signal reception cutoff threshold δ (determined based on the hardware used and environment) such that if the signal strength is below δ , the channel is in the OFF state. Moreover, in order to adequately capture the dynamics of the mmWave channels, the timeout value T_{out} is set on-the-fly such that at time t , we set $T_{out}(t) = \bar{Z}_{RF}(t)$ with $\bar{Z}_{RF}(t)$ to be the RF average waiting time. Thus, on average, packets would not get stuck in the mmWave queue longer than if they would have joined the RF queue.

Optimality results: We first investigate the tradeoff between mmWave throughput (or, conversely, *link wastage*) and the



(a) Throughput performance



(b) Delay performance

Fig. 11. Throughput and delay performance of our proposed threshold based policy compared with the Backpressure policy under real-time and delayed CSI conditions.

average waiting time. Link wastage is defined as the fraction of time slots that there are packets in the system, but the mmWave queue is empty and the mmWave link is available (i.e., $L(t) = 1$). The tradeoff between link wastage and the average waiting time is shown in Fig. 10(a). From the results, we observe that if there are so many packets added to the mmWave queue and if the mmWave link becomes unavailable, high average delay incurs. On the other hand, a conservative policy is not desirable either such that due to lack of packets in the mmWave queue, the link wastage increases. Figure 10(b) illustrates the total reward obtained as a function of the admission threshold where the maximum reward is obtained for threshold 11, which is the same threshold value with zero link wastage and the smallest average waiting in Fig. 10(a).

Comparison with Backpressure: Backpressure algorithms promise optimal throughput performance for a wide range of networking problems [15]. However, it is well-known that they suffer from high end-to-end packet delay. Figure 11 demonstrates the throughput and delay performance of our threshold-based scheduler compared with the Backpressure algorithm applied for the network model in Fig. 7 under both real-time CSI and delayed CSI conditions. From the results, we observe that the threshold-based scheme achieves a similar throughput performance compared with the Backpressure, while delay is mostly enhanced and is bounded. It should be noted that the threshold-based scheme does not require explicit knowledge of the CSI since due to the high data rate of the mmWave interface, real-time tracking of the CSI may not be feasible.

VI. CONCLUSION

In this paper, we proposed a hybrid communications architecture for 5G cellular systems in which the mmWave and RF

interfaces are integrated in a coherent fashion. Our proposed architecture includes an RF-assisted beamforming that exploits the correlation between the RF and mmWave interfaces in order to enhance the energy and delay overhead of mmWave beamforming. In addition to beamforming, we proposed the use of RF interface for data transfer, and formulated an optimal scheduling policy in order to maximize the long-term throughput of the mmWave interface provided that the average delay is bounded. We cast the constrained throughput maximization as a *reward optimization*, and proved that the optimal scheduling policy has a simple monotone structure. As a result, using the RF interface as a secondary data transfer mechanism, the abundant yet intermittent mmWave bandwidth is fully exploited. Indeed, we believe that mmWave will most likely be deployed with an overlay of RF in 5G.

ACKNOWLEDGMENT

This work was supported in part by the following grants from the National Science Foundation CNS-1618566 and CNS-1421576.

REFERENCES

- [1] F. Khan and Z. Pi, "mmWave mobile broadband (MMB): Unleashing the 3–300GHz spectrum," in *34th IEEE Sarnoff Symposium*, 2011.
- [2] T. S. Rappaport, S. Sun, R. Mayzus, H. Zhao, Y. Azar, K. Wang, G. N. Wong, J. K. Schulz, M. Samimi, and F. Gutierrez, "Millimeter wave mobile communications for 5G cellular: It will work!" *Access, IEEE*, vol. 1, pp. 335–349, 2013.
- [3] W. Roh, J.-Y. Seol, J. Park, B. Lee, J. Lee, Y. Kim, J. Cho, K. Cheun, and F. Aryanfar, "Millimeter-wave beamforming as an enabling technology for 5G cellular communications: theoretical feasibility and prototype results," *IEEE Communications Magazine*, vol. 52, no. 2, 2014.
- [4] J. Mo, A. Alkhateeb, S. Abu-Surra, and R. W. Heath Jr, "Hybrid architectures with few-bit ADC receivers: Achievable rates and energy-rate tradeoffs," *arXiv preprint arXiv:1605.00668*, 2016.
- [5] T. Nitsche, A. B. Flores, E. W. Knightly, and J. Widmer, "Steering with eyes closed: mm-wave beam steering without in-band measurement," in *Computer Communications (INFOCOM), IEEE Conference on*. IEEE, 2015, pp. 2416–2424.
- [6] A. Ali, N. González-Prelcic, and R. W. Heath Jr, "Estimating millimeter wave channels using out-of-band measurements," 2016.
- [7] S. Collonge, G. Zaharia, and G. E. Zein, "Influence of the human activity on wide-band characteristics of the 60 GHz indoor radio channel," *Wireless Communications, IEEE Transactions on*, vol. 3, no. 6, pp. 2396–2406, 2004.
- [8] A. Adhikary, E. Al Safadi, M. K. Samimi, R. Wang, G. Caire, T. S. Rappaport, and A. F. Molisch, "Joint spatial division and multiplexing for mm-wave channels," *IEEE Journal on Selected Areas in Communications*, vol. 32, no. 6, pp. 1239–1255, 2014.
- [9] Y. Kim, K. Lee, and N. B. Shroff, "An analytical framework to characterize the efficiency and delay in a mobile data offloading system," in *Proceedings of the 15th ACM international symposium on Mobile ad hoc networking and computing*. ACM, 2014, pp. 267–276.
- [10] J. G. Andrews, T. Bai, M. Kulkarni, A. Alkhateeb, A. Gupta, and R. W. Heath Jr, "Modeling and analyzing millimeter wave cellular systems," *arXiv preprint arXiv:1605.04283*, 2016.
- [11] R. Schmidt, "Multiple emitter location and signal parameter estimation," *IEEE transactions on antennas and propagation*, vol. 34, no. 3, pp. 276–280, 1986.
- [12] M. L. Puterman, *Markov decision processes: discrete stochastic dynamic programming*. John Wiley & Sons, 2014.
- [13] M. Larrañaga, O. J. Boxma, R. Núñez-Queija, and M. S. Squillante, "Efficient content delivery in the presence of impatient jobs," in *Teletraffic Congress (ITC 27), 27th International*. IEEE, 2015, pp. 73–81.
- [14] M. Hashemi, C. E. Koksall, and N. B. Shroff, "Hybrid RF-mmWave communications to achieve low latency and high energy efficiency in 5g cellular systems," *arXiv preprint arXiv:1701.06241*, 2017.
- [15] L. Georgiadis, M. J. Neely, and L. Tassiulas, *Resource allocation and cross-layer control in wireless networks*. Now Publishers Inc, 2006.